Promising Ferroelectricity in 2D Group IV Tellurides: a First-Principles Study

Wenhui Wan, ^{1, a)} Chang Liu, ^{1, a)} Wende Xiao, ¹ and Yugui Yao^{1, b)} Beijing Key Laboratory of Nanophotonics and Ultrafine Optoelectronic Systems, School of Physics, Beijing Institute of Technology, Beijing 100081, China.

(Dated: 20 July 2017)

Based on the first-principles calculations, we investigated the ferroelectric properties of two-dimensional (2D) Group-IV tellurides XTe (X=Si, Ge and Sn), with a focus on GeTe. 2D Group-IV tellurides energetically prefer an orthorhombic phase with a hinge-like structure and an in-plane spontaneous polarization. The intrinsic Curie temperature T_c of monolayer GeTe is as high as 570 K and can be raised quickly by applying a tensile strain. An out-of-plane electric field can effectively decrease the coercive field for the reversal of polarization, extending its potential for regulating the polarization switching kinetics. Moreover, for bilayer GeTe the ferroelectric phase is still the ground state. Combined with these advantages, 2D GeTe is a promising candidate material for practical integrated ferroelectric applications.

PACS numbers: 77.80.-e, 77.80.bn, 77.80.Fm, 77.80.B-Keywords: Two-dimensional ferroelectricity, Strain engineering, Curie point, Coercive field

Nanoscale devices based on ferroelectric thin films and compatible with Si chips have many potential applications, e.g. ultrafast switching, cheap room-temperature magnetic-field detectors, electrocaloric coolers for computers and nonvolatile random access memories.^{1–3} However, it is still a great challenge to keep the ferroelectricity stable in thin films at room temperature to date.⁴ For the conventional ferroelectric materials such as BaTiO₃ or PbTiO₃, the enhanced depolarization field will destroy the ferroelectricity at critical thicknesses of about 12 Å and 24 Å,^{5,6} respectively. To address this challenge, new two-dimensional (2D) ferroelectric phases with ferroelectricity sustained against such a depolarization field are desirable to pave the way for the application of "integrated ferroelectrics".

Compared with their bulk counterparts, 2D materials often lose some symmetry elements (e.g. centrosymmetry) as the result of dimensionality reduction, ^{7,8} which favors the appearance of ferroelectricity. A number of 2D ferroelectric phases have been theoretically proposed, e.g. the distorted 1T MoS₂ monolayer, 9 low-buckled hexagonal IV-III binary monolayers including InP and AsP, ¹⁰ unzipped graphene oxide monolayer ¹¹ and monolayer Group-IV monochalcogenides. 12-14 The Group-IV monochalcogenides including GeS, GeSe, SnS and SnSe have attracted much attention due to their large in-plane spontaneous polarizations P_s in theory ¹⁴ and experimental accessibility. Monolayers of SnSe and GeSe have been successfully synthesized. 15,16 However, the ground-state SnSe and GeSe multilayers adopt a stacking order that the directions of P_s in two neighboring layers are opposite.¹³ Thus, the non-zero polarization only exists in odd-numbered layers, hindering their ferroelectric applications. Excitingly, a robust ferroelectricity has been experimentally observed in SnTe(001) few-layers. To Compared with the low Curie temperature $T_c = 98$ K in bulk SnTe, 18 the T_c in monolayer SnTe was greatly enhanced to 270 K, due to the suppression of the Sn-vacancy and the in-plane expansion of the lattice. 4,17 Meanwhile, the P_s in 2D SnTe are aligned along the in-plane < 110 > direction, in contrast to the < 111 > direction in bulk. 19 This behavior again indicates that the dimensionality reduction favors the formation of new ferroelectric phases. However, the ferroelectric properties of 2D SnTe predicted in

a) These two authors contributed equally

b) Electronic mail: ygyao@bit.edu.cn

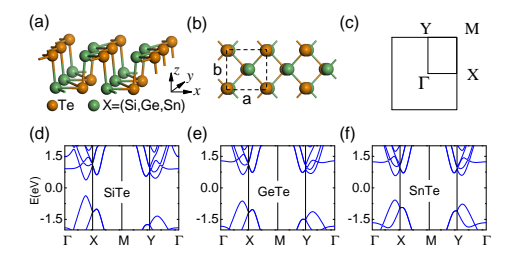


FIG. 1. (a, b) Side and top views of the crystal structure of monolayer XTe (X=Si, Ge and Sn), respectively. (c) 2D first Brillouin zone. (d-f) Band structures of monolayer SiTe, GeTe and SnTe, respectively.

theory are inconsistent with the experimental measurements.¹⁷ This calls for a microscopic understanding of the relevant physics. Additionally, the discovery of the ferroelectricity in 2D SnTe shades light on the possible ferroelectric phase in other Group-IV tellurides. Bulk GeTe is ferroelectric and exhibits a rhombohedral crystal structure.²⁰ No crystal phase has been identified in bulk SiTe, but several thermodynamically stable phases of 2D SiTe have been theoretically proposed.²¹ To date, the ferroelectric properties of both 2D GeTe and 2D SiTe remain unexplored.

In this work, we investigated the structural, electronic and ferroelectric properties of 2D Group-IV tellurides XTe (X=Si, Ge and Sn). All computational details are in the supplementary material (SM).²² We found that 2D Group-IV tellurides prefer a hinge-like structure with an in-plane spontaneous polarization. During the reversal of polarization, monolayer SiTe undergoes a semiconductor-to-metal transition, while monolayer GeTe and SnTe keep semiconducting and ferroelectric. Monolayer GeTe has a high ferroelectricity transition T_c of 570 K. However, for 2D SnTe, the achievement of the room-temperature ferroelectricity requires external strain. The ferroelectricity of 2D GeTe can be effectively controlled through the application of strain engineering and vertical electric fields. Moreover, bilayer GeTe exhibits a ferroelectric ground state that the polarization of each layer is aligned parallel. These novel properties provide 2D GeTe a promising material for future nanoscale ferroelectric applications.

Though bulk GeTe and SnTe adopt a rhombohedral structure below the Curie temperature, 18,20 the synthesized 2D SnTe exhibits a layered orthorhombic phase with a hinge-like structure. The corresponding monolayer is displayed in Fig. 1(a) and 1(b). Each of the four atoms in a unit cell is three-fold coordinated with the atoms of the other species. a and b are the lattice vectors along the x (puckered) and y (zigzag) directions, respectively. We first calculated the crystal structure of the monolayer SnTe with different methods to ensure the reliability of our simulations. The theoretical results as well as the experimental data relisted in the Table S1 of SM. In the special hinge-like structure of monolayer SnTe, some atoms are close to each other without covalent bonding (see Fig. 1(a)). The distance between them is larger than 3.2 Å. Description of this kind of interaction due to the weak wave function overlap should include the vdW interactions, which have been reported in the phosphorene. Considering the lattice anisotropy which is critical in the determining the ferroelectricity, it was found that the optPBE-vdW method produces the best results (see Table S1²²) compared with the experiment.

Based on this method, the optimized lattice constants of monolayer Group-IV tellurides are given in Table I. No imaginary frequency is observed in the phonon dispersions (see Fig. S1²²), confirming their structural stability. Additionally, it is found the orthorhombic phase of monolayer Group-IV tellurides is more stable than the hexagonal phase extracted from the bulk (see the Fig. S2 and Table S2 of SM^{22}), in line with the previous theoretical work²⁵ and the experiment.¹⁷

The calculated band structures of monolayer Group-IV tellurides are shown in Figs. 1(d-f). The trend of the band gaps is $E_g(\text{GeTe}) > E_g(\text{SnTe}) > E_g(\text{SiTe})$. The anomalous order of E_g might be the result of the fine balance between the relative atomic energy levels

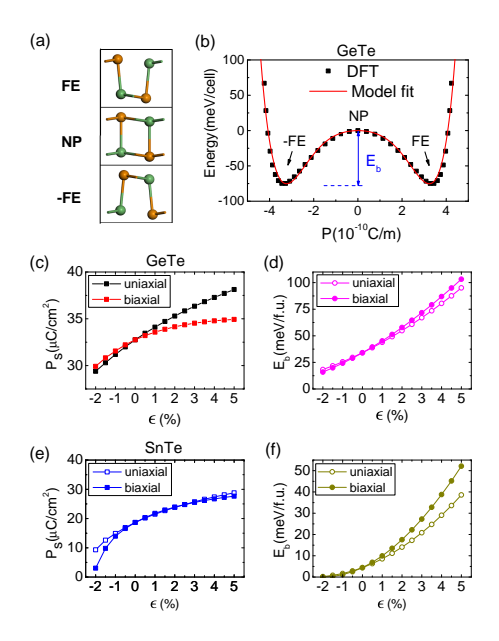


FIG. 2. (a) Two symmetry-equivalent ferroelectric states with opposite in-plane polarizations as well as a high-symmetry, non-polar transition state. (b) Double-well potential of monolayer GeTe vs polarization. E_b is the ferroelectric transition barrier. The red line represents the fitting curve of the Landau-Ginzburg model. The uniaxial and biaxial strains dependence of P_s and E_b for (c, d) monolayer GeTe and (e, f) monolayer SnTe, respectively.

and the repulsion between the levels²⁶ The anisotropy of the band structure and phonon dispersion decreases from monolayer SiTe to monolayer SnTe, consistent with the decrease of the anisotropy of their lattice constants (see Table I).

In such an orthorhombic structure, the Group-IV atoms displace along the x-direction with respect to the Te atoms, leading to the break of the centrosymmetry but the perseveration of the yz-mirror symmetry. Spontaneous polarization is aligned along the x-direction and can be labeled as a scalar P_s . Therefore, the thickness of 2D ferroelectric Group-IV tellurides will not be limited by the aforementioned depolarization field vertical to the slab, ^{5,6} but another lateral critical size still exists due to the in-plane depolarization field. ¹⁴ The polarization P_s was calculated by the Berry phase approach.²⁷ The reversal of polarization is realized through a phase transition between two symmetry-equivalent ferroelectric states with opposite P_s (labeled as the FE state and -FE state in Fig. 2(a)). By calculating the transition barrier E_b of several pathways using the nudged-elastic-band (NEB) methods,²⁸ we found that a transition path through a centrosymmetric non-polar (NP) state (see Fig. 2(a)) has the lowest E_b . With this transition path, we calculated the polarization dependence of free energy F(P) and show the result specific to monolayer GeTe in Fig. 2(b). The P_s in the FE state is 3.28×10^{-10} C/m, equivalent to a bulk polarization of 32.8 μ C/cm² if an effective thickness of 1 nm for monolayer GeTe is used. The transition barrier E_b is estimated by the energy difference between the FE and NP states (see

TABLE I. The lattice constants (a, b), lattice anisotropy $\delta = (\frac{a}{b} - 1) \times 100\%$, intrinsic polarization P_s and ferroelectric transition barrier E_b of monolayer SiTe, GeTe and SnTe.

	a (Å)	b (Å)	$\delta(\%)$	$P_s(\mu { m C/cm}^2)$	$E_b(\mathrm{meV/f.u.})$
SiTe	4.452	4.127	7.88	42.0	88.5
GeTe	4.472	4.273	4.66	32.8	37.4
SnTe	4.666	4.577	1.95	19.4	4.48

Fig. 2(b)). For monolayer GeTe, E_b is 74.8 meV, equivalent to 37.4 meV per formula unit (f.u.) and much smaller than $E_b \approx 200 \text{ meV/f.u.}$ in conventional ferroelectric PbTiO₃.²⁹ This small E_b indicates that the required electric field for the reversal of polarization in monolayer GeTe would be much lower than that in PbTiO₃.

The ferroelectricity can be substantially affected by the external strain.³⁰ Here the strain is defined as $\epsilon = (\frac{a}{a_0} - 1) \times 100\%$ where a and a_0 are the lattice constants along the x- or y-direction for the strained and unstrained structures, respectively. It is found that both uniaxial (ϵ_x) and biaxial (ϵ_x) tensile strains can enlarge the displacement of the Ge atoms with respect to the Te atoms and therefore effectively enhance the P_s and E_b of monolayer GeTe, as shown in Figs. 2(c, d). In contrast, the compressive strain suppresses the P_s and E_b .

Monolayer SnTe has a larger P_s and higher E_b than that of GeTe (see Table I). However, its band gap calculated using HSE06 approach³¹ will be closed during the reversal of P_s (see Fig. S3²²), leading to a drop of P_s to zero. This semiconductor-metal transition hinders the ferroelectric application of 2D SiTe, but make 2D SiTe suited for the field effect switching devices.³²

Monolayer SnTe remains semiconducting during the reversal of P_s . The effective P_s and the E_b of monolayer SnTe is small (see Table I). After applying a tensile strain, both P_s and E_b can be effectively increased (Figs. 2(e, f)), showing that the ferroelectricity of 2D SnTe can be effectively tuned by strain.

The stability of ferroelectricity is represented by the Curie temperatures T_c at which the macroscopic spontaneous polarization vanishes. Based on the Landau-Ginzburg phase transition theory, 13,33 the free energy of GeTe supercell is written as a Taylor expansion in terms of the polarization:

$$F = \sum_{i} \left(\frac{A}{2} P_i^2 + \frac{B}{4} P_i^4 + \frac{C}{6} P_i^6 \right) + \frac{D}{2} \sum_{\langle i,j \rangle} (P_i - P_j)^2, \tag{1}$$

where P_i is the polarization of each unit cell. The first three terms describe the anharmonic double-well potential in a unit cell (see Fig. 2(b)). The last term represents the dipole-dipole interaction between the nearest neighboring unit cells. The parameter D can be estimated by a fitting process in the mean-field approximation.¹³ All the fitted parameters are given in the Table S3 of SM.²² The Monte Carlo simulations were performed with the effective Hamiltonian of Eq. 1 to investigate the ferroelectric phase transition. As shown in Fig. 3(a), the T_c of unstrained monolayer GeTe is 570 K. By applying a biaxial strain of 2%, the T_c can be easily enhanced to 903 K, as illustrated in Fig. 3(b), consistent with the increase of the transition barrier E_b (see Fig. 2(d)).

In contrast, the T_c of unstrained monolayer SnTe is only 166 K (see Fig. 3(b)), much smaller than the experimental value of $T_c=270$ K. ¹⁷ However, the T_c can be increased quickly by applying a biaxial tensile strain (see Fig. 3(b)). The sensitive response of the ferroelectricity to external strain in 2D SnTe offers a possible reason to explain the difference between the predicted T_c and experimental one. The theoretical lattice anisotropy δ of monolayer SnTe is 1.95% (see Table. I) which is smaller than the experimental $\delta=3.15\%$. ¹⁷ If an uniaxial tensile strain of $\epsilon_x=1.0\%$ is applied to monolayer SnTe, the T_c can be enhanced from 166 K to 265 K, close to the experimental T_c of 270 K. ¹⁷ The external strain has also been observed in other materials in the vdW epitaxy, ^{34–36} such as GaSe flakes via vdW epitaxy on the Si (111) surface. ³⁴ The origin of strain in 2D SnTe calls for a future study.

The averaged polarization $\langle P_i \rangle$ in the vicinity of the T_c follows an asymptotic form^{13,37} of $\langle P_i \rangle = C(T_c - T)^{\delta}$ with $T < T_c$. Here, C is a constant and δ is the critical exponent. For monolayer GeTe, the asymptotic form fits well with the MC simulations, as shown in Fig. 3(a). P_s decreases continuously to zero at T_c . The δ is 0.195, deviating from δ =0.5 in the second-order ferroelectric phase transition.³⁷ A similar behavior has also been reported in other IV-VI compounds such as SnSe.¹³

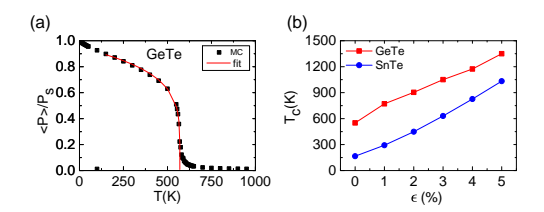


FIG. 3. (a) Temperature dependence of averaged polarization $\langle P_i \rangle$ of monolayer GeTe obtained by the MC simulations. Here the $\langle P_i \rangle$ at different temperature has been normalized with respect to the $\langle P_i \rangle_{T=0K} = P_s$. The red line represents a fitting curve of P_s with an asymptotic form in the vicinity of the Curie temperatures T_c . (b) Biaxial strain dependence of T_c for monolayer GeTe (red line) and SnTe (blue line).

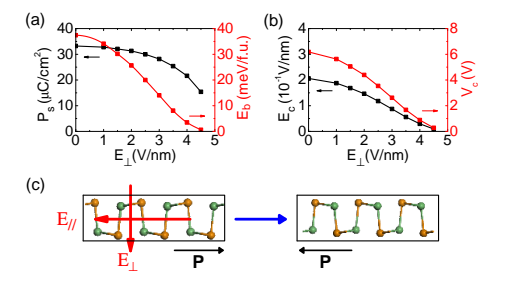


FIG. 4. (a) Vertical electric field E_{\perp} dependence of polarization P_s and transition barrier E_b of monolayer GeTe. (b) Vertical electric field E_{\perp} dependence of in-plane coercive field E_c and coercive voltage V_c of monolayer GeTe. (c) A schematic representation of the switching of polarization of monolayer GeTe by a combination of an in-plane electric field $E_{//}$ and an out-of-plane electric field E_{\perp} .

Based on the Landau-Ginzburg phase transition theory,³³ the electric field E can be calculated from free energy, i.e. $E = \frac{\partial F(P)}{\partial P}$. The coercive field E_c is at the turning points of the hysteresis loop P(E), satisfying the condition of $(\frac{\partial P}{\partial E})^{-1}|_{E=E_c}=0$. Therefore, the ideal E_c can be estimated from the maximum slope of the F(P) curve between the NP and FE states.¹⁴ A lateral size of l=30 nm is adopted to estimate the effective coercive voltage $V_c=lE_c$. This lateral size is about the one of latest ferroelectric field effect transistor memory.³⁸ Through the F(P) curve of monolayer GeTe (Fig. 2(b)), the estimated E_c is 0.206 V/nm and the effective V_c is 6.18 V. It is noted that the ideal E_c of the bulk ferroelectric material is always much higher than the experimentally measured E_c , due to the growth and propagation of the ferroelectric domains.³⁹ However, the distinction between them at the nanoscale become small as thin ferroelectric films turn out to be more homogeneous than bulk and the formation of ferroelectric domains is suppressed.^{37,40}

It is found that if a vertical electric field E_{\perp} was applied, the in-plane displacements of the Ge atoms with respect to the Te atoms will decrease, due to the field-induced coulomb forces. This leads to a reduction of the P_s and E_b (see Fig. 4(a)). As a result, the in-plane coercive field E_c in monolayer GeTe can be effectively decreased by E_{\perp} , as displayed in Fig. 4(b). The maximum E_{\perp} required to tune the E_c is about 4.5 V/nm (see Fig. 4(b). The equivalent V_{\perp} is 4.5 V if an effective thickness of 1 nm for monolayer GeTe is adopted. Fig. 4(c) depicts a feasible way for fast switching the polarization by a combination of two mutually perpendicular electric fields. In this switching process, the required operating voltages are less than 5V, which is desirable for the integration into Si-based semiconducting devices.^{2,3}

The stacking order is crucial for the ferroelectricity of multilayers of Group-IV tellurides. We first defined two kinds of stacking order for bilayer GeTe, namely, AA and anti-AA stacking. As shown in Fig. 5(a), for AA-stacking, the top layer is directly stacked on top of the bottom layer, so that polarization of each layer is aligned parallel. By further shifting

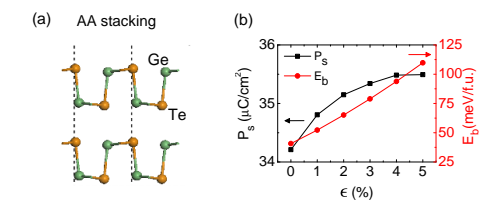


FIG. 5. The (a) AA stacking order for bilayer GeTe. (b) Biaxial strain dependence of the P_s and E_b of bilayer GeTe with the AA stacking.

the top layer of AA-stacking with a/2, b/2 and (a+b)/2, we can get other three stacking orders labeled as AB, AC and AD stacking. The anti-AA stacking can be gotten if the top layer of the AA-stacked bilayer is rotated around the z axis by 180°. Other stacking orders, e.g. anti-AB, anti-AC and anti-AD can be obtained with a similar process. The energies of bilayer GeTe with different stacking order are shown in Table S4.²² The bilayer GeTe with the AA stacking has the lowest energy. The effective thickness of bilayer GeTe is taken as the twice of that of its monolayer. The corresponding effective bulk P_s and E_b is $34.2~\mu\text{C/cm}^2$ and 40.1~meV/f.u., respectively, exhibiting a increase compared with that of monolayer GeTe (see Fig. 2(c) and Fig. 5(d)). Tensile strain can further enhance the P_s and E_b of bilayer GeTe (see Fig. 5(d)). Thus, the promising ferroelectricity also exists in bilayer GeTe.

For bilayer SnTe, the AA-stacking is also the ground state but exhibits a weak ferroelectricity (see Table S4²²). Therefore, 2D GeTe and SnTe take the advantage over aforementioned Group-IV monochalcogenides such as SnSe in ferroelectric application, as the ferroelectricity in 2D SnSe only exists in odd-numbered layers.¹³

In summary, we show by the first-principles calculations that 2D GeTe with a hinge-like crystal structure is ferroelectric with an in-plane spontaneous polarization. When examining the atomic structure and ferroelectricity of 2D GeTe, it is necessary to include of the van der Waals interactions in order to well describe the interatomic interactions. The Curie temperatures T_c of monolayer GeTe is as high as 570 K. Tensile strain can effectively enhance the T_c and serves as a powerful tool to improve the ferroelectricity of 2D GeTe. The in-plane coercive field for reversing the polarization can be widely tuned by a vertical electric field, facilitating the fast switching of polarization. Furthermore, for bilayer GeTe the ferroelectric phase is still the ground state. With these advantages, 2D GeTe may be the long-sought candidate for realizing the integrated ferroelectric applications.

We acknowledge professor Wei Kang (Peking university) and Dr. Ruixiang Fei (Washington University) for their fruitful discussions. The work is supported by the National Natural Science Foundation of China (Grant No. 11574029) and the MOST Project of China (Nos. 2014CB920903, 2016YFA0300600).

¹L. W. Martin and A. M. Rappe, "Thin-film ferroelectric materials and their applications," Nat. Rev. Mater. 2, 16087 (2016).

²M. Dawber, K. M. Rabe, and J. F. Scott, "Physics of thin-film ferroelectric oxides," Rev. Mod. Phys. **77**, 1083–1130 (2005).

³J. F. Scott, "Applications of modern ferroelectrics," Science **315**, 954–959 (2007).

⁴B. J. Kooi and B. Noheda, "Ferroelectric chalcogenides—materials at the edge," Science **353**, 221–222 (2016).

⁵J. Junquera and P. Ghosez, "Critical thickness for ferroelectricity in perovskite ultrathin films," Nature 422, 506–509 (2003).

⁶D. D. Fong, G. B. Stephenson, S. K. Streiffer, J. A. Eastman, O. Auciello, P. H. Fuoss, and C. Thompson, "Ferroelectricity in ultrathin perovskite films," Science **304**, 1650–1653 (2004).

⁷X. Xu, W. Yao, D. Xiao, and T. F. Heinz, "Spin and pseudospins in layered transition metal dichalcogenides," Nat. Phys. 10, 343–350 (2014).

⁸M. N. Blonsky, H. L. Zhuang, A. K. Singh, and R. G. Hennig, "Ab initio prediction of piezoelectricity in two-dimensional materials," ACS Nano 9, 9885–9891 (2015).

⁹S. N. Shirodkar and U. V. Waghmare, "Emergence of ferroelectricity at a metal-semiconductor transition in a 1t monolayer of mos₂," Phys. Rev. Lett. **112**, 157601 (2014).

- ¹⁰D. Di Sante, A. Stroppa, P. Barone, M.-H. Whangbo, and S. Picozzi, "Emergence of ferroelectricity and spin-valley properties in two-dimensional honeycomb binary compounds," Phys. Rev. B 91, 161401 (2015).
- ¹¹M. Noor-A-Alam and Y.-H. Shin, "Switchable polarization in an unzipped graphene oxide monolayer," Phys. Chem. Chem. Phys. 18, 20443–20449 (2016).
- ¹²M. Wu and X. C. Zeng, "Intrinsic ferroelasticity and/or multiferroicity in two-dimensional phosphorene and phosphorene analogues," Nano Lett. **16**, 3236–3241 (2016).
- ¹³R. Fei, W. Kang, and L. Yang, "Ferroelectricity and phase transitions in monolayer group-iv monochalco-genides," Phys. Rev. Lett. **117**, 097601 (2016).
- ¹⁴H. Wang and X. Qian, "Two-dimensional multiferroics in monolayer group iv monochalcogenides," 2D Materials 4, 015042 (2017).
- ¹⁵L. Li, Z. Chen, Y. Hu, X. Wang, T. Zhang, W. Chen, and Q. Wang, "Single-layer single-crystalline snse nanosheets," J. Am. Chem. Soc. 135, 1213–1216 (2013).
- ¹⁶Y. Sun, Z. Sun, S. Gao, H. Cheng, Q. Liu, F. Lei, S. Wei, and Y. Xie, "All-surface-atomic-metal chalcogenide sheets for high-efficiency visible-light photoelectrochemical water splitting," Adv. Energy Mater. 4, 1300611 (2014).
- ¹⁷K. Chang, J. Liu, H. Lin, N. Wang, K. Zhao, A. Zhang, F. Jin, Y. Zhong, X. Hu, W. Duan, Q. Zhang, L. Fu, Q.-K. Xue, X. Chen, and S.-H. Ji, "Discovery of robust in-plane ferroelectricity in atomic-thick snte," Science 353, 274–278 (2016).
- ¹⁸M. Iizumi, Y. Hamaguchi, K. F. Komatsubara, and Y. Kato, "Phase transition in snte with low carrier concentration," J. Phys. Soc. Jpn. 38, 443–449 (1975).
- ¹⁹E. Plekhanov, P. Barone, D. Di Sante, and S. Picozzi, "Engineering relativistic effects in ferroelectric snte," Phys. Rev. B 90, 161108 (2014).
- ²⁰D. Di Sante, P. Barone, R. Bertacco, and S. Picozzi, "Electric control of the giant rashba effect in bulk gete," Adv. Mater. 25, 509–513 (2013).
- ²¹Y. Chen, Q. Sun, and P. Jena, "Site monolayers: Si-based analogues of phosphorene," J. Mater. Chem. C 4, 6353–6361 (2016).
- ²²See Supplemental Material at for the structural and energetical properties of monolayer and bilayer Group IV Tellurides, the fitted parameters for the effective Hamiltonian, the phonon dispersion of monolayer Group IV Tellurides and semiconductor-metal transition in monolayer SiTe.
- ²³ J. Qiao, X. Kong, Z.-X. Hu, F. Yang, and W. Ji, "High-mobility transport anisotropy and linear dichroism in few-layer black phosphorus," Nature communications 5 (2014).
- ²⁴J. Klimeš, D. R. Bowler, and A. Michaelides, "Van der waals density functionals applied to solids," Phys. Rev. B 83, 195131 (2011).
- ²⁵A. K. Singh and R. G. Hennig, "Computational prediction of two-dimensional group-iv monochalcogenides," Appl. Phys. Lett. 105, 042103 (2014).
- ²⁶S.-H. Wei and A. Zunger, "Electronic and structural anomalies in lead chalcogenides," Phys. Rev. B 55, 13605–13610 (1997).
- ²⁷R. D. King-Smith and D. Vanderbilt, "Theory of polarization of crystalline solids," Phys. Rev. B 47, 1651–1654 (1993).
- ²⁸G. Henkelman, B. P. Uberuaga, and H. Jnsson, "A climbing image nudged elastic band method for finding saddle points and minimum energy paths," J. Chem. Phys. 113, 9901–9904 (2000).
- ²⁹R. E. Cohen, "Origin of ferroelectricity in perovskite oxides," Nature **358**, 136–138 (1992).
- ³⁰ J. H. Haeni, P. Irvin, W. Chang, R. Uecker, P. Reiche, Y. L. Li, S. Choudhury, W. Tian, M. E. Hawley, B. Craigo, A. K. Tagantsev, X. Q. Pan, S. K. Streiffer, L. Q. Chen, S. W. Kirchoefer, J. Levy, and D. G. Schlom, "Room-temperature ferroelectricity in strained srtio3," Nature 430, 758–761 (2004).
- ³¹ J. Paier, M. Marsman, K. Hummer, G. Kresse, I. C. Gerber, and J. G. Ángyán, "Screened hybrid density functionals applied to solids," J. Chem. Phys. 124, 154709 (2006).
- ³²Z. Yang, C. Ko, and S. Ramanathan, "Oxide electronics utilizing ultrafast metal-insulator transitions," Annu. Rev. Mater. Res. 41, 337–367 (2011).
- ³³R. Cowley, "Structural phase transitions i. landau theory," Adv. Phys. **29**, 1–110 (1980).
- ³⁴H. Cai, E. Soignard, C. Ataca, B. Chen, C. Ko, T. Aoki, A. Pant, X. Meng, S. Yang, J. Grossman, F. D. Ogletree, and S. Tongay, "Band engineering by controlling vdw epitaxy growth mode in 2d gallium chalcogenides," Adv. Mater. 28, 7375–7382 (2016).
- ³⁵Y. Wang, Y.-Y. Sun, S. Zhang, T.-M. Lu, and J. Shi, "Band gap engineering of a soft inorganic compound pbi2 by incommensurate van der waals epitaxy," Appl. Phys. Lett. 108, 013105 (2016).
- ³⁶K. Zhang, S. Hu, Y. Zhang, T. Zhang, X. Zhou, Y. Sun, T.-X. Li, H. J. Fan, G. Shen, X. Chen, and N. Dai, "Self-induced uniaxial strain in mos2 monolayers with local van der waals-stacked interlayer interactions," ACS Nano 9, 2704–2710 (2015).
- ³⁷V. Fridkin and S. Ducharme, "The ferroelectricity at the nanoscale," Ferroelectrics **466**, 133–144 (2014).
- ³⁸S. Mueller, S. Slesazeck, S. Henker, S. Flachowsky, P. Polakowski, J. Paul, E. Smith, J. Mller, and T. Mikolajick, "Correlation between the macroscopic ferroelectric material properties of si:hfo2 and the statistics of 28 nm fefet memory arrays," Ferroelectrics 497, 42–51 (2016).
- ³⁹S. Kim, V. Gopalan, and A. Gruverman, "Coercive fields in ferroelectrics: A case study in lithium niobate and lithium tantalate," Appl. Phys. Lett. 80, 2740–2742 (2002).
- ⁴⁰M. J. Highland, T. T. Fister, M.-I. Richard, D. D. Fong, P. H. Fuoss, C. Thompson, J. A. Eastman, S. K. Streiffer, and G. B. Stephenson, "Polarization switching without domain formation at the intrinsic

coercive field in ultrathin ferroelectric $\mathrm{pbtio}_3, \mathrm{"Phys.~Rev.~Lett.~} \mathbf{105},\, 167601$ (2010).